

# Synthesis, characterization and formation mechanism of quasi-spherical $\text{Gd}_2\text{O}_2\text{S}:\text{Pr}^{3+}$ phosphor by sulfurization of oxide powder using ammonium thiocyanate and argon gas

HUILIN QU<sup>1,2</sup>, JINGBAO LIAN<sup>1,1,\*</sup>, NIANCHU WU<sup>1,2</sup>, XUE ZHANG<sup>1,2</sup>, JIAO HE<sup>1,2</sup>

<sup>1</sup>School of Mechanical Engineering, Liaoning Petrochemical University, Fushun, 113001, P.R. China

<sup>2</sup>New Functional Materials Laboratory, Liaoning Petrochemical University, Fushun, 113001, P.R. China

Quasi-spherical  $\text{Gd}_2\text{O}_2\text{S}:\text{Pr}^{3+}$  green phosphor was successfully synthesized via sulfurization of oxide powders using ammonium thiocyanate and argon gas. XRD analysis shows that the  $\text{Gd}_2\text{O}_2\text{S}$  powder is pure phase after calcination and sulfurization. FE-SEM shows that the precursor can eventually be transformed into quasi-spherical  $\text{Gd}_2\text{O}_2\text{S}$  powder with an average size of 150 nm. Moreover, the formation mechanism of  $\text{Gd}_2\text{O}_2\text{S}$  has also been proposed. PL analysis shows that the emission spectrum of  $\text{Gd}_2\text{O}_2\text{S}:1.00\%\text{Pr}^{3+}$  exists strong green emission band centered at 513 nm upon excitation at 460 nm light, and its corresponding CIE coordinate is (0.331, 0.564).

(Received October 19, 2021; accepted August 10, 2022)

**Keywords:** Rare earth oxysulfide, Phosphors, Sulfurization, Ammonium thiocyanate, Photoluminescence

## 1. Introduction

Rare-earth oxide sulfides, commonly named oxysulfides in the literature[1] ( $\text{Ln}_2\text{O}_2\text{S}$ , Ln standing here for rare-earth) are materials of undeniable promising from both in performance and application. Due to their closed-shell electron configuration[2], rare-earth elements such as Y, La, Gd, and Lu can be selected to form  $\text{Ln}_2\text{O}_2\text{S}$  host materials that can then be doped by another lanthanide[3]. The rare-earth oxysulfide phosphors generally show excellent luminescent performances, good chemical stability[4], high X-ray conversion efficiency, short attenuation time, and innocuity[5], thus these phosphors have been widely used in multi-faces: medical diagnostic imaging, radiation detectors for high-energy physics, radiation monitoring, and environmental applications[6].

In numerous experiments and explorations by scientists have shown that when Gd is the main body, its comprehensive performance is good.  $\text{Gd}_2\text{O}_2\text{S}$  has a hexagonal crystal structure[7], wide band gap (4.6-4.8eV)[8], high density ( $7.34\text{g}\cdot\text{cm}^{-3}$ )[9], good chemical stability and high X-ray blocking ability[10]. Hard radiation stability and high density ( $7.34\text{g}\cdot\text{cm}^{-3}$ ) makes it an effective trap of the incident X-ray photon. Thus, in recent years,  $\text{Gd}_2\text{O}_2\text{S}$  has gradually entered people's field of vision, which has attracted extensive

attention. For instance:  $\text{Gd}_2\text{O}_2\text{S}:\text{Pr}^{3+}$  with one-dimensional (1D) structures have been studied for potential applications in television screens[11], cathode ray tubes[12], and X-ray intensifying screens[13].

At present, the usual synthesis of  $\text{Gd}_2\text{O}_2\text{S}$  materials consists of solid state reactions under quite severe experimental conditions. Solid state synthesis is also a common preparation method, usually through the addition of flux, for example,  $\text{Na}_2\text{CO}_3$ ,  $\text{K}_2\text{CO}_3$ ,  $\text{Li}_2\text{PO}_4$  to prepare  $\text{Gd}_2\text{O}_2\text{S}$ . However, this method needs to solve such problems as controlling the size uniformity, monodispersity and crystallinity[14]. Moreover, several methods have been reported, such as, hydrothermal and solvothermal methods[15], combustion synthesis[16] and oxide sulfurization[17]. Hydrothermal and solvothermal methods are widely used in the synthesis of rare earth oxysulfides because the nanometer rare earth oxysulfides can be obtained directly by changing the solvent. The combustion method has the advantages of short reaction time, high purity and small particle size. It is an effective way to prepare  $\text{Gd}_2\text{O}_2\text{S}$ , but this method may increase the surface defects and agglomerate. Though some of the above mentioned methods were able to produce fine particles/crystallites of uniform sizes, they have the disadvantages of either complicated procedure, low yield, production of waste gas, generation of toxic gas and high cost. The traditional sulfurization method will melt and

destroy the morphology of rare earth oxides[18]. Ammonium thiocyanate is used as sulfur source and the pyrolysis end point is 724.35 °C in argon atmosphere[19]. The gas products may be HNCS, NH<sub>3</sub>, CS<sub>2</sub> and H<sub>2</sub>S. In this paper, we propose to use ammonium thiocyanate sulfurization method to synthesize Gd<sub>2</sub>O<sub>2</sub>S. It not only overcomes the problems of toxicity, safety and cost caused by traditional sulfurization of hydrogen sulfide, carbon disulfide and sublimation sulfur, but also has the advantages of low calcination temperature, low cost and a friendly environment.

## 2. Experimental

### 2.1. Synthesis

Gadolinium oxide (Gd<sub>2</sub>O<sub>3</sub>, AR), praseodymium nitrate (Pr(NO<sub>3</sub>)<sub>3</sub>·6H<sub>2</sub>O, 99.99% purity), nitric acid (HNO<sub>3</sub>, AR), ammonia (NH<sub>3</sub>·H<sub>2</sub>O), urea (CO(NH<sub>2</sub>)<sub>2</sub>, AR) and ammonium thiocyanate (NH<sub>4</sub>SCN, AR) were used as the starting materials without further purification. Gd<sub>2</sub>O<sub>3</sub> and Pr(NO<sub>3</sub>)<sub>3</sub>·6H<sub>2</sub>O were purchased from Jining Tianyi New Material Co. Ltd, China. Urea and ammonia were purchased from Sinopharm Chemical Reagent Co. Ltd, China. Ammonium thiocyanate was purchased from Wuxi Yatai United Chemical Co. Ltd, China. Typical homogeneous precipitation synthesis of Gd<sub>2</sub>O<sub>3</sub> and sulfurization procedure of preparing Gd<sub>2</sub>O<sub>2</sub>S phosphor

was indicated below. Firstly, 0.5 mol·L<sup>-1</sup> Gd(NO<sub>3</sub>)<sub>3</sub> stock solution was prepared by dissolving a certain amount of Gd<sub>2</sub>O<sub>3</sub> powder in dilute nitric acid solution, meanwhile, concentrated ammonia was added to adjust the pH of the solution to 4.82. Then 500 mL Gd(NO<sub>3</sub>)<sub>3</sub> solution with 0.01 mol·L<sup>-1</sup> was prepared, and a certain amount of Pr(NO<sub>3</sub>)<sub>3</sub>·6H<sub>2</sub>O was weighed to prepare Pr(NO<sub>3</sub>)<sub>3</sub> solution with a concentration of 10 mmol·L<sup>-1</sup>. According to the molar ratio (u) of urea:gadolinium nitrate=10, 20, 30, 40:1, 3g, 6g, 9g and 12g urea were dissolved in Gd(NO<sub>3</sub>)<sub>3</sub> solution and stirred until completely dissolved. The above solution was heated in a water bath at 90 °C for 2h and aged. Then the obtained turbid liquid was washed with deionized water and absolute ethanol for many times, filtered, and dried in a vacuum drying oven at 80 °C for 12 h to obtain the precursor. The precursor was calcined in muffle furnace at different temperatures for 2 h to obtain the final product Gd<sub>2</sub>O<sub>3</sub> powder. Pr<sup>3+</sup> doped precursors with different molar concentrations were also prepared by the same process. Here, Pr<sup>3+</sup> concentration is 0.10%, 0.25%, 0.50%, 1.00%, 1.50% and 2.00%, respectively. Ammonium thiocyanate was heated at 450 °C in argon atmosphere to produce sulfurization atmosphere, and then a certain amount of Gd<sub>2</sub>O<sub>3</sub> powder was put into corundum firing boat, and then sulfurized in the tubular furnace at different temperatures (600-750 °C) for 1h to obtain Gd<sub>2</sub>O<sub>2</sub>S target product. The experimental flow chart is shown in Fig. 1.

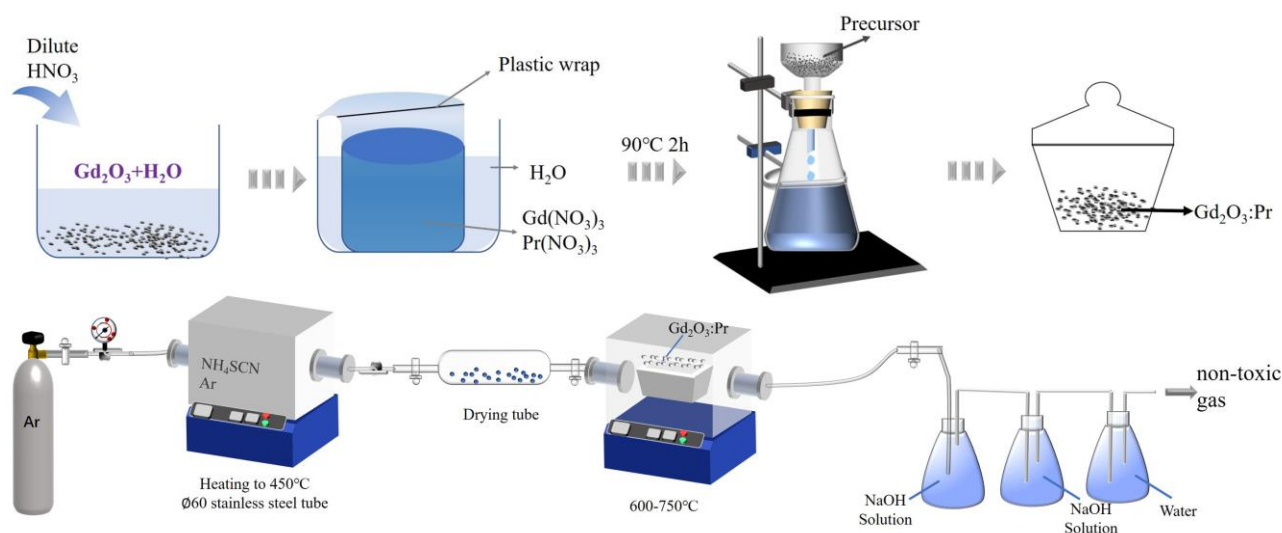


Fig. 1. Schematic illustration for the preparation process of Gd<sub>2</sub>O<sub>2</sub>S:Pr<sup>3+</sup> phosphors (color online)

### 2.2. Characterization

X-ray diffraction (XRD) measurements were carried out using a D8 Advance XRD diffractometer with CuK<sub>α</sub> radiation of 0.15406 nm, and the operation voltage and current were kept at 40 kV and 30 mA, respectively. In

data acquisition, the 2θ value is 10° to 90°. The morphology of the as-prepared samples was determined using a field emission scanning electron microscope (FE-SEM, Hitachi SU8000). Agilent Cary 660 fourier transform infrared spectrometer (FT-IR) was used to determine the chemical structure of the substance

through the infrared light absorbed by the vibration in the chemical bond by the KBr method. Simultaneous differential thermal analysis (DSC-TG) was carried out using a SDT 2960 thermal analyzer in flowing air at a heating rate of  $5\text{ }^\circ\text{C}\cdot\text{min}^{-1}$ . Photoluminescence (PL) spectra and decay time were obtained on a Hitachi F-7000 fluorescence spectrophotometer equipped with IBH TemPro fluorescence lifetime measurement system.

### 3. Results and discussion

#### 3.1. Morphology analysis of the synthetic products

As mentioned above, we prepared the precursors of urea and gadolinium nitrate according to the molar ratio of  $u=10, 20, 30$  and  $40$  respectively, and analyzed the precursors and their corresponding calcined products by FE-SEM, as shown in Fig. 2. It can be clearly seen that all the four precursors are spherical with slight agglomeration, wherein the  $u=40$  precursor has a uniform spherical structure with good dispersion and the average size of the precursor is approximately  $300\text{ nm}$ . While the morphology contours of all the four precursors were well maintained with a slight shrinkage in size after the calcination treatment at  $1000\text{ }^\circ\text{C}$ , we can see that its average size is approximately  $150\text{--}200\text{ nm}$  (Fig. 2d<sub>2</sub>). It can be seen from Fig.2 that the morphologies of the calcined products are almost the same. However, according to the yield of the precursors, we found that the higher the  $u$  value is, the higher the yield is, finally we chose the  $u$  value of  $40$  in the present study.

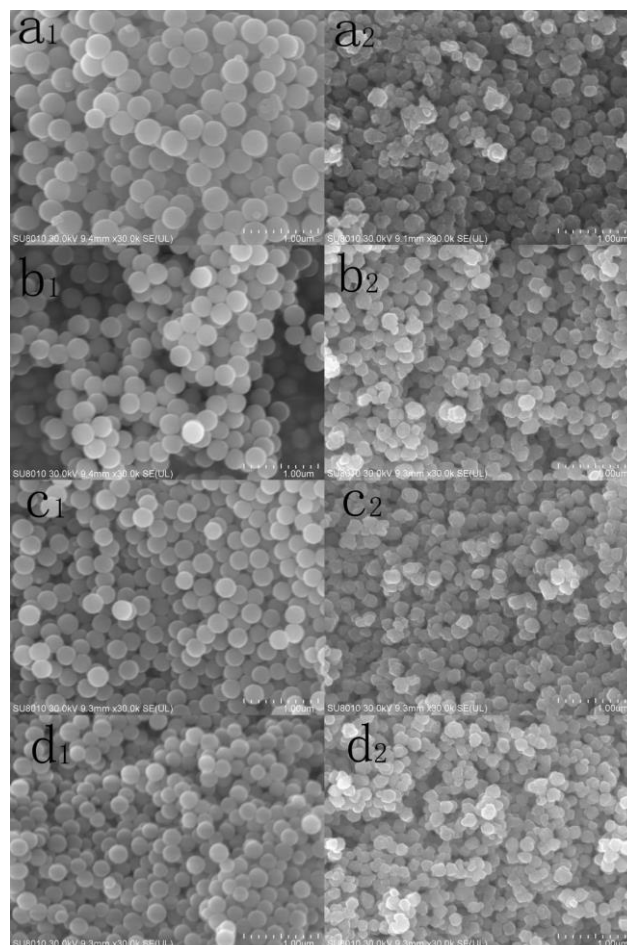


Fig. 2. FE-SEM images of the precursors and their corresponding calcined products synthesized with different  $u$  values (The precursor: a<sub>1</sub>  $u=10$ ; b<sub>1</sub>  $u=20$ ; c<sub>1</sub>  $u=30$ ; d<sub>1</sub>  $u=40$ ; The calcined products: a<sub>2</sub>  $u=10$ ; b<sub>2</sub>  $u=20$ ; c<sub>2</sub>  $u=30$ ; d<sub>2</sub>  $u=40$ )

#### 3.2. Thermal decomposition behavior of the precursor

To understand the decomposition behavior and determine the calcination temperature for the precursor, DSC-TG-DTG of the precursor with  $u=40$  was conducted from room temperature to  $1300\text{ }^\circ\text{C}$  and the results are shown in Fig. 3. Three steps of weight loss are observed in TG curve of precursor. The first gradual weight loss at  $184\text{ }^\circ\text{C}$  is attributed to the thermal decomposition of anhydrous ethanol and evaporation of adsorbed water with a weight loss rate of  $4.47\%$ . This weight loss corresponds to a weak endothermic peak at around  $137\text{ }^\circ\text{C}$  in the DSC curve, and DTG maxima at about  $156\text{ }^\circ\text{C}$  in the DTG curve. The second sharp weight loss in the temperature range of  $184\text{ }^\circ\text{C}$  to  $600\text{ }^\circ\text{C}$  may be ascribed to decomposition of crystal water and dehydrogenation of hydroxyl water with the weight loss rate of  $17.09\%$ ,

and no obvious endothermic peak in the DSC curve. The last weight loss starting at  $\sim 600$  °C is associated with the complete decomposition of  $\text{CO}_3^{2-}$  groups of the precursor. At the same time, this weight loss accompanies with an obvious exothermic peak at around 605 °C in the DSC curve, and a strong peak at about 600 °C in the DTG

curve. Moreover, as shown in Fig. 3, little weight changes can be observed at temperatures greater than 1000 °C on the TG curve, which indicates that the thermal decomposition is basically finished at 1000 °C in the present study.

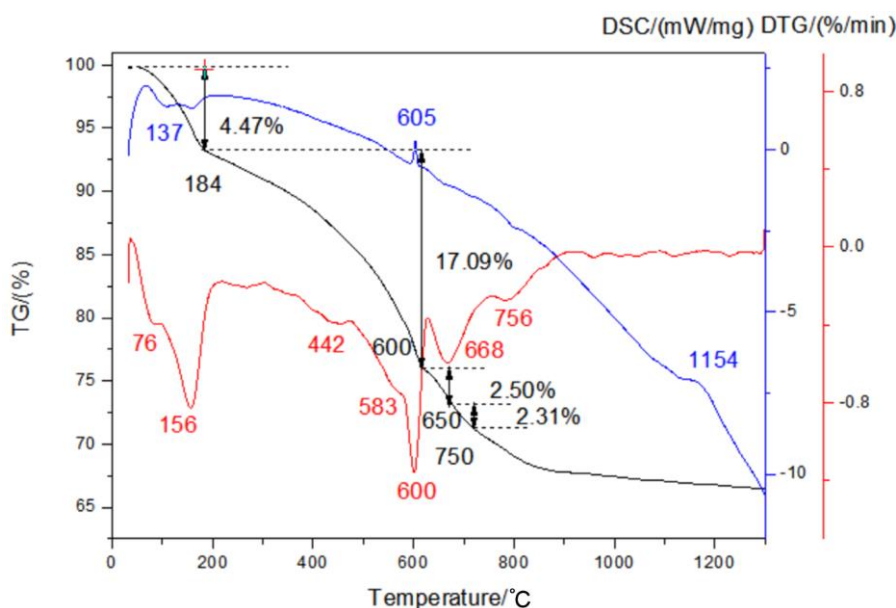


Fig. 3. DSC-TG-DTG curves of the precursor between room temperature and 1300 °C (color online)

### 3.3. Phase and structure analysis

Based on  $u=40$ , the precursor was calcined at different temperatures for many times. Finally, the products calcined at 400 °C and 1000 °C were analyzed by XRD. It can be seen from Fig. 4a that the precursor is amorphous in structure with essentially no diffraction peaks. After 400 °C calcination (Fig. 4b), no obvious change was observed in the calcination product compared with its precursor, in other words, the calcined product still remains amorphous structure. When the calcination temperature is 1000 °C, the diffraction pattern has obvious diffraction peaks (Fig. 4c). Compared with JCPDS standard card 01-088-2165 (Fig. 4d), it is found that all diffraction peaks can be indexed as pure  $\text{Gd}_2\text{O}_3$  phase and the as prepared powder shows good crystallinity, so we finally choose the calcination temperature of 1000 °C.

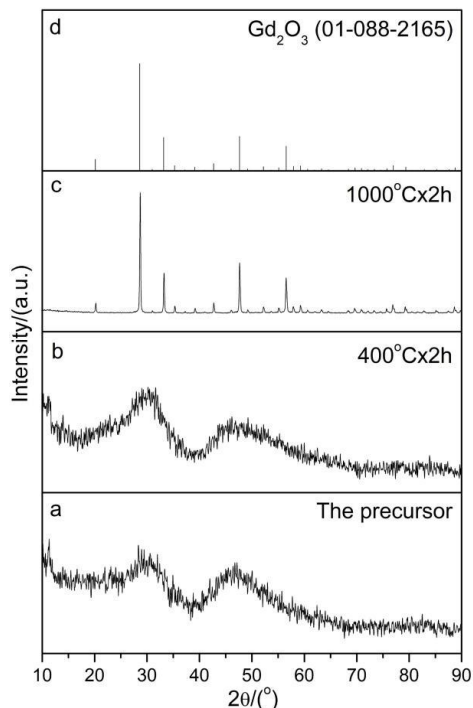


Fig. 4. XRD patterns of the precursor synthesized by  $u=40$  and its products calcined at different temperatures

The as prepared  $\text{Gd}_2\text{O}_3$  powder was then sulfurized at different temperatures in tube furnace. Here, the sulfurization atmosphere was obtained by heating ammonium thiocyanate in argon gas flow, and then XRD was used for phase analysis. Fig. 5 shows XRD patterns of the  $\text{Gd}_2\text{O}_3$  powder sulfurized at different temperatures. It can be clearly seen that the XRD diffraction pattern of Fig. 5.a exists sharp peaks. Compared with JCPDS standard card 00-026-1422 (Fig. 5 b), all the XRD diffraction peaks don't exactly match, indicating that there are heterophases. What's more, according to Fig. 5 c, the  $2\theta=28.54^\circ$  and  $2\theta=33.13^\circ$  peaks recorded in Fig. 5 a can be indexed to  $\text{Gd}_2\text{O}_3$  trace impurities (JCPD no. 01-0880-2165). In other words, sulfurization of  $\text{Gd}_2\text{O}_3$  powder at  $600^\circ\text{C}$  yields hexagonal  $\text{Gd}_2\text{O}_2\text{S}$  as predominant phase with trace  $\text{Gd}_2\text{O}_3$  as impurities. With continuously increasing the sulfurization temperature to  $650^\circ\text{C}$ , the sharp peaks of Fig. 5 d are compared with JCPDS standard card (00-026-1422), which indicates that the sulfurized product consists of pure  $\text{Gd}_2\text{O}_2\text{S}$  phase. In the same way, we can see from Fig. 5 e that there are some disordered diffraction peaks when the sulfurization temperature is  $700^\circ\text{C}$ . Compared with the standard card of  $\text{Gd}_2\text{S}_3$  (JCPDS no.00-045-0985) (Fig. 5 f), there are several consistent peaks, indicating that the sulfurization product is composed of the mixture of  $\text{Gd}_2\text{S}_3$  and  $\text{Gd}_2\text{O}_2\text{S}$ . A further increasing temperature of  $750^\circ\text{C}$  results in the formation of pure  $\text{Gd}_2\text{S}_3$  phase owing to complete sulfurization reaction of  $\text{Gd}_2\text{O}_3$ . From the above sulfurization temperature, we can see that  $650^\circ\text{C}$  is appropriate sulfurization temperature for synthesizing pure  $\text{Gd}_2\text{O}_2\text{S}$  phase.

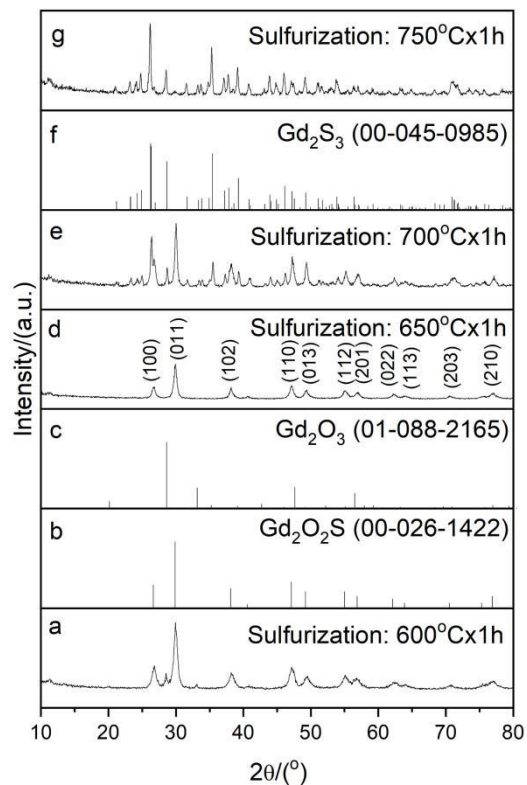


Fig. 5. XRD patterns of the  $\text{Gd}_2\text{O}_3$  powder sulfurized at different temperatures: (a)  $600^\circ\text{C}$ ; (b) XRD standard pattern of  $\text{Gd}_2\text{O}_2\text{S}$ ; (c) XRD standard pattern of  $\text{Gd}_2\text{O}_3$ ; (d)  $650^\circ\text{C}$ ; (e)  $700^\circ\text{C}$ ; (f) XRD standard pattern of  $\text{Gd}_2\text{S}_3$ ; (g)  $750^\circ\text{C}$  (color online)

### 3.4. Morphology analysis of the sulfurization products

Fig. 6 shows FE-SEM images of the  $\text{Gd}_2\text{O}_3$  powder sulfurized at different temperatures. From Fig. 6 a it's obvious that when the sulfurization temperature is  $600^\circ\text{C}$ , the obtained product is near sphere in shape and the particle size is between 100-200 nm. In addition, the aggregation of particle is light, and the distance between particles is far from each other. It's can be clearly seen that when the sulfurization temperature is  $650^\circ\text{C}$ , the as synthesized  $\text{Gd}_2\text{O}_2\text{S}$  particle has a quasi spherical structure with an average size is approximately 150 nm and exhibit smooth surfaces, but is slightly agglomerated from Fig.6b. However, when the temperature raised to 700 and  $750^\circ\text{C}$ , it's obvious from Fig. 6 c and Fig. 6 d that the sphericity of particles after sulfurization was almost impossible to be seen, with sizes ranging from 400 nm to 600 nm, and severe adhesion to each other, which could not reach the expected spherical state.

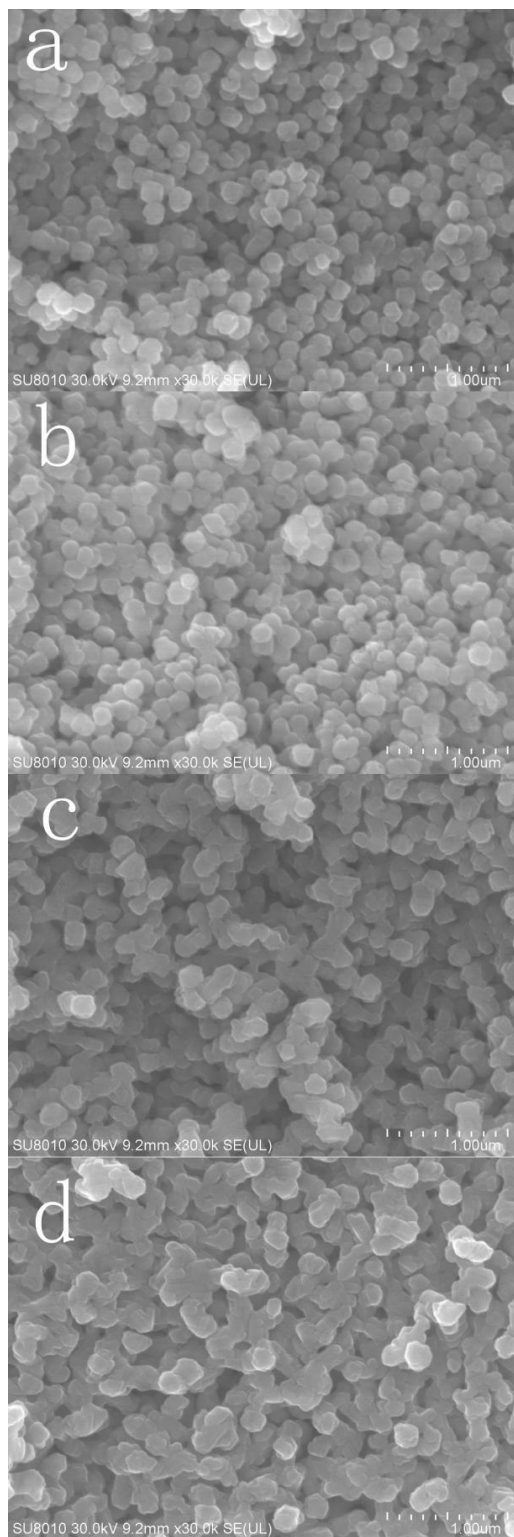


Fig. 6. FE-SEM images of  $Gd_2O_3$  synthesized by  $u=40$  and its products vulcanized at different temperatures (a) 600 °C; (b) 650 °C; (c) 700 °C; (d) 750 °C

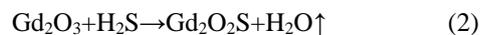
### 3.5. Formation mechanism of the synthetic products

According to the literature[20-21], the pyrolysis end point of ammonium thiocyanate in an argon atmosphere is 724.35 °C, and the pure ammonium thiocyanate will be isomerized into thiourea at 140 °C. When the temperature rises to 450 °C, the -SCN and C-S absorption bands almost disappear and virtually complete desulfurization occurs, the band of  $C\equiv N$  trimerizes and vanishes, then the band of C-N and  $C=N$  is rebuilt. Ammonium bisulfate can construct triazine ring system through spin, polymerization and condensation process, and release ammonia ( $NH_3$ ) and hydrogen sulfide ( $H_2S$ ) at the same time. And the decomposition reaction can be expressed as follows (1):



Moreover, the yellowish residue remains after the  $NH_4SCN$  heated at 450 °C in argon atmosphere, which is found to be graphitic carbon nitride ( $g-C_3N_4$ ) by XRD analysis. As shown in Fig. 7, there are two characteristic peaks located at  $2\theta=27.1^\circ$  and  $13.5^\circ$ ; their crystal planes are (002) and (100), respectively, when  $2\theta=27.1^\circ$  is the strongest diffraction peak,  $d=0.329$  nm. It is due to the characteristic of conjugate direction system, which is interlayer stacking reflection. In addition, another significant diffraction peak locates at  $2\theta=13.5^\circ$ ,  $d=0.675$  nm, which belongs to the regular arrangement of triazine rings in the carbon nitride plane.

According to the above analysis, the gas products of ammonium thiocyanate in thermal decomposition process are  $NH_3$  and  $H_2S$ , among which  $H_2S$  can be used as sulfurization reagent, and reacts with gadolinium oxide ( $Gd_2O_3$ ) in argon atmosphere to form gadolinium oxysulfide ( $Gd_2O_2S$ ), which proceeds according to the following reaction (2):



In sum, the schematic diagram of the experimental reaction mechanism (Fig. 7) corresponds well to the above analysis.

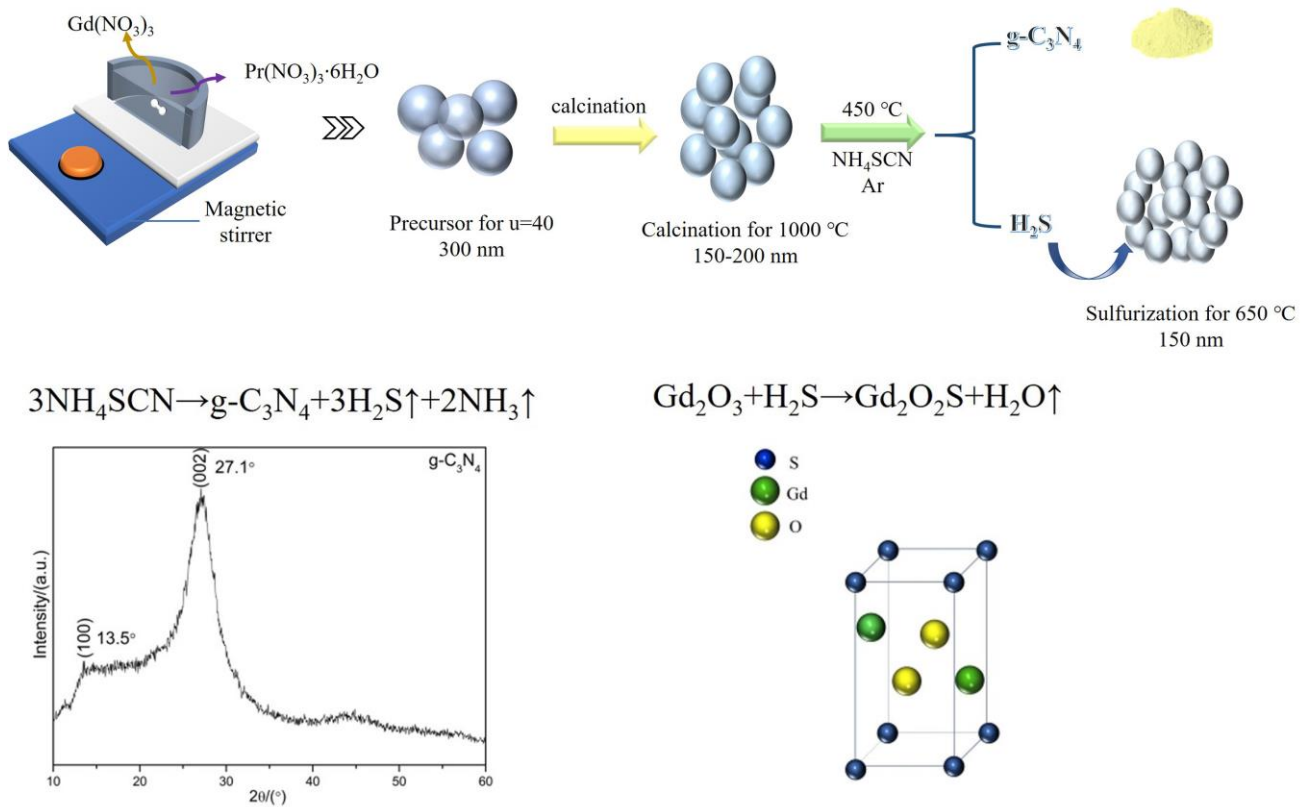


Fig. 7. Schematic diagram of formation mechanism for the Gd<sub>2</sub>O<sub>2</sub>S (color online)

### 3.6. Photoluminescence properties

Fig. 8 shows the excitation and emission spectra of Gd<sub>2</sub>O<sub>2</sub>S:x%Pr<sup>3+</sup> phosphor. From Fig. 8, we can see that the intensity of the excitation emission spectra are all maximum when the doping concentration is 1.00%. In Fig. 8a, when the excitation wavelength is less than 270 nm, the absorption peak intensity is obviously enhanced, which is due to the host lattice absorption of Gd<sub>2</sub>O<sub>2</sub>S. It is well established that the peak wavelength of luminescence depends on the band gap, we also can prove by formula:

$$E_g = 1240/\lambda(\text{eV}) \quad (3)$$

when  $\lambda = 270$  nm,  $E_g = 4.593$  eV, which is in good agreement with the band gap of Gd<sub>2</sub>O<sub>2</sub>S (4.6 eV). Pr<sup>3+</sup> is prone to 4f<sup>2</sup>→4f5d transition and fluorescence, and its emission spectrum is wide diffuse band (wide absorption band), it can be observed that there exists two broad band

excitation peaks in the range of 275 nm-500 nm, and the one around 300 nm in the longer wavelength region, corresponding to the 4f<sup>2</sup>→4f5d transition of Pr<sup>3+</sup> ions. The other around 460 nm is attributed to <sup>3</sup>H<sub>j</sub>→<sup>3</sup>P<sub>j</sub>, <sup>1</sup>I<sub>6</sub> transition of Pr<sup>3+</sup> ions. Fig. 8 b shows the emission spectrum of Gd<sub>2</sub>O<sub>2</sub>S:1.00%Pr<sup>3+</sup> phosphor upon excitation at 460 nm of blue light. One can see that the green and weak red emission bands centered around 550, 675 and 770 nm. The strongest green emission band centered at 513 nm belongs to the <sup>3</sup>P<sub>0</sub>→<sup>3</sup>H<sub>4</sub> energy level transitions of Pr<sup>3+</sup> ions, and the weak red emission is assigned to the transition of <sup>3</sup>P<sub>0</sub>→<sup>3</sup>H<sub>6</sub>, <sup>3</sup>P<sub>0</sub>→<sup>3</sup>F<sub>2</sub> and <sup>3</sup>P<sub>0</sub>→<sup>3</sup>F<sub>3</sub>, <sup>3</sup>F<sub>4</sub> energy level transitions of Pr<sup>3+</sup> ions.

To make sure the maximum doping concentration of Gd<sub>2</sub>O<sub>2</sub>S:x%Pr<sup>3+</sup> phosphors, we doped a series of Pr<sup>3+</sup> to Gd<sub>2</sub>O<sub>2</sub>S:x%Pr<sup>3+</sup> phosphors. Fig. 9 shows the curve of the influence of the concentration of Pr<sup>3+</sup> doping on the luminescent intensity of Gd<sub>2</sub>O<sub>2</sub>S:x%Pr<sup>3+</sup> phosphors and its corresponding Log (I/C) and Log (C) fitting curve. Fig. 9 a presents a plot of the intensity curve of the

concentration of  $\text{Pr}^{3+}$  ions. We can see that when the concentration of  $\text{Pr}^{3+}$  is between 0.10% and 0.25%, the luminescent intensity of  $\text{Gd}_2\text{O}_2\text{S}:x\%\text{Pr}^{3+}$  phosphors increases slowly.

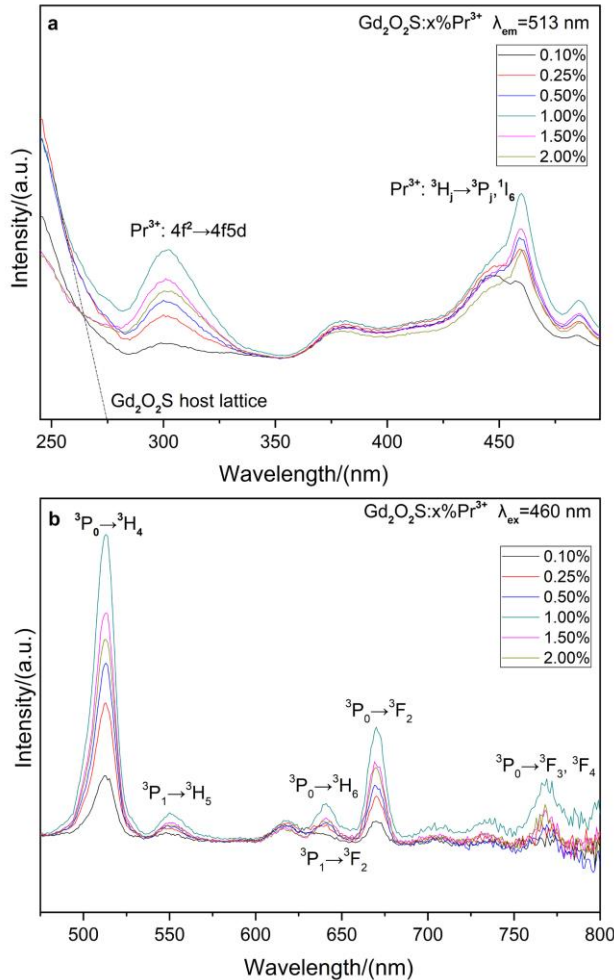


Fig. 8. (a) Excitation and (b) emission spectra of  $\text{Gd}_2\text{O}_2\text{S}:x\%\text{Pr}^{3+}$  phosphor (color online)

While when the concentration of  $\text{Pr}^{3+}$  is between

0.25% and 0.50%, the luminescent intensity of  $\text{Gd}_2\text{O}_2\text{S}:x\%\text{Pr}^{3+}$  phosphors increases rapidly, then when the concentration of  $\text{Pr}^{3+}$  is 1.00%, the intensity is the highest value. When the concentration of  $\text{Pr}^{3+}$  is higher than 1.00%, the luminescence intensity of  $\text{Gd}_2\text{O}_2\text{S}:x\%\text{Pr}^{3+}$  phosphors continues to decline. When the concentration of  $\text{Pr}^{3+}$  is 1.50% and 2.00%, both have very close intensity. According to Dexter's theory, the luminescence intensity is related to the doping concentration of activator. The relationship of concentration can be expressed by the following formula:

$$\log(I/C) = (-s/d) \log C + \log f \quad (4)$$

where  $d$  is 3,  $C$  is the doping concentration, and  $f$  is a constant independent of the doping concentration. When  $s=3, 6, 8$  and  $10$ , the mechanism of concentration quenching is exchange interaction, electric dipole-electric dipole, electric dipole-electric quadrupole and electric quadrupole-electric quadrupole interaction, respectively. By fitting the high concentration point in Fig. 9 b, the fitting curve is

$$\log(I/C) = -0.7945 \log(C) + 2.9321 \quad (5)$$

The slope parameter  $-s/d$  was determined to be  $-0.7945$  (close to  $-1$ ), thus yielding an  $s$  value of 3. This indicates that the exchange interaction is the concentration quenching mechanism for the  ${}^3P_0 \rightarrow {}^3H_4$  transition of  $\text{Pr}^{3+}$  ions in the  $\text{Gd}_2\text{O}_2\text{S}:x\%\text{Pr}^{3+}$  phosphors.

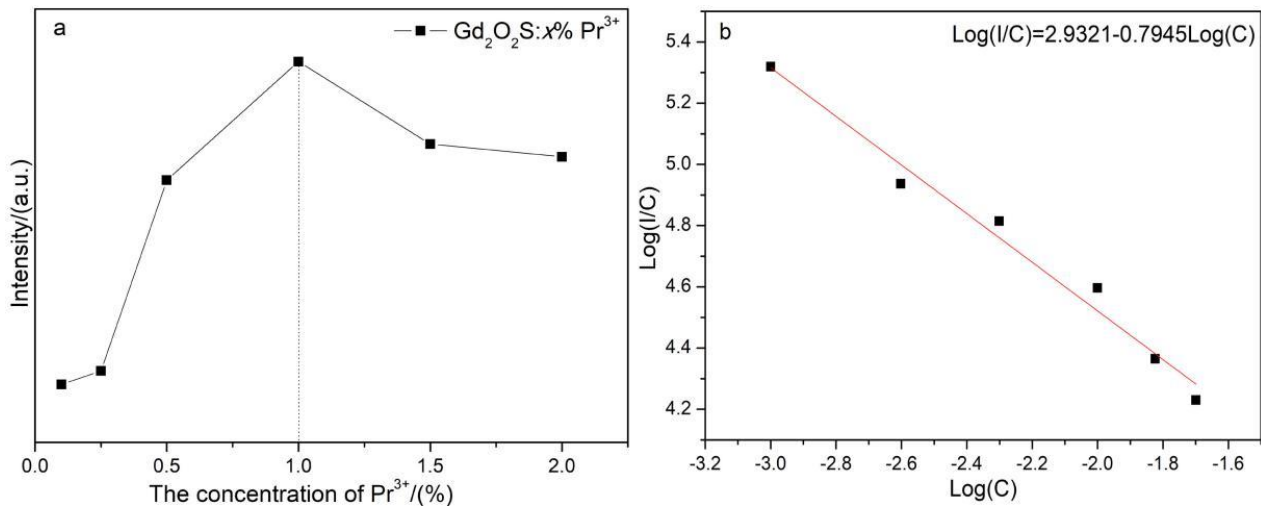


Fig. 9. (a) Concentration quenching curve and (b) quenching mechanism of  $\text{Gd}_2\text{O}_2\text{S}:\text{x}\%\text{Pr}^{3+}$  phosphors (color online)

In 1931, CIE stipulated that the basis of XYZ color system was equal color experiment, and the viewing angle was  $2^\circ$ , which was smaller than the actual viewing angle of judging color. Therefore, on this basis, the chromaticity chart of  $10^\circ$  test sites appeared in 1964. To figure out the emission color composition with different doping concentrations of  $\text{Pr}^{3+}$ , here we employ the CIE chromaticity diagram to calculate the green emission and the results are shown in Fig. 10. It can be clearly seen that the color tone of samples changes from yellow-green (0.356, 0.548) to light-yellow green (0.332, 0.563) by doping different concentrations of  $\text{Pr}^{3+}$ .

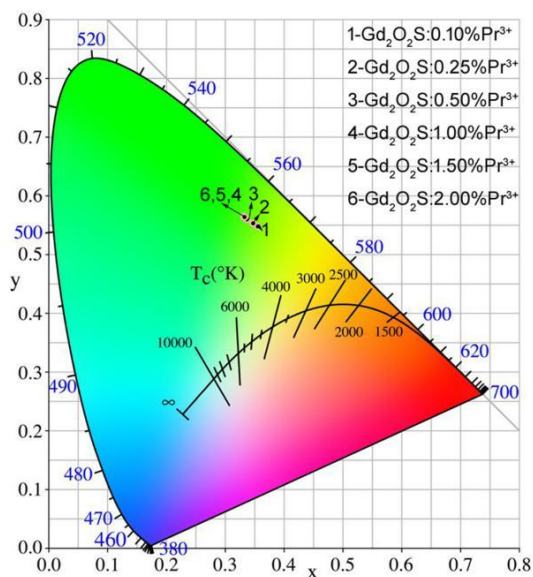


Fig. 10. CIE coordinate diagram of  $\text{Gd}_2\text{O}_2\text{S}:\text{x}\%\text{Pr}^{3+}$  phosphors (color online)

Table 1 shows the coordinates of  $\text{Gd}_2\text{O}_2\text{S}:\text{x}\%\text{Pr}^{3+}$  ( $\text{x}=0.10, 0.25, 0.50, 1.00, 1.50$  and  $2.00$ ) phosphor are (0.356, 0.548), (0.348, 0.553), (0.337, 0.560), (0.331, 0.564), (0.332, 0.564) and (0.332, 0.563), which correspond to  $\text{Pr}^{3+}$  ions concentrations of 0.10%, 0.25%, 0.50%, 1.00%, 1.50% and 2.00%, respectively. Based on the above analysis, it is obviously found that the emission colors of  $\text{Gd}_2\text{O}_2\text{S}:\text{x}\%\text{Pr}^{3+}$  phosphors are tunable by changing the concentration of  $\text{Pr}^{3+}$  ions, which is considered to be a promising candidate for application in the fields of green light emitting devices.

Table 1. CIE coordinates of  $\text{Gd}_2\text{O}_2\text{S}:\text{x}\%\text{Pr}^{3+}$  phosphors

| $\text{Pr}^{3+}(\%)$ | CIE <sub>x</sub> | CIE <sub>y</sub> | Peak | Peak Intensity |
|----------------------|------------------|------------------|------|----------------|
| 0.10                 | 0.356            | 0.549            | 513  | 208            |
| 0.25                 | 0.348            | 0.554            | 513  | 220            |
| 0.50                 | 0.338            | 0.560            | 513  | 326            |
| 1.00                 | 0.331            | 0.565            | 513  | 395            |
| 1.50                 | 0.332            | 0.564            | 513  | 347            |
| 2.00                 | 0.333            | 0.564            | 513  | 340            |

#### 4. Conclusions

A homogeneous precipitation followed by a sulfurization route has been successfully developed for synthesizing pure quasi-spherical  $\text{Gd}_2\text{O}_2\text{S}:\text{Pr}^{3+}$  green phosphor, which adopts ammonium thiocyanate as

sulfurization reagent of and argon as carrier gas. When  $u=40$ , the precursor has uniform spherical structure with good dispersion and the average size of the precursor is approximately 300 nm. The  $Gd_2O_3$  powder with quasi-spherical structure can be obtained by calcination at 1000 °C for 2 h in air. Through a series of sulfurization experiments in this work, it is finally concluded that pure  $Gd_2O_2S$  phase could be prepared at 650 °C for 1 h under argon and  $H_2S$  environment. The morphology of  $Gd_2O_2S$  is quasi-spherical in shape and the particle average size is about 150 nm. The as synthesized  $Gd_2O_2S:Pr^{3+}$  phosphors exhibit green emission at 513 nm upon excitation at 460 nm of blue light, corresponding to the  $^3P_0 \rightarrow ^3H_4$  transition of  $Pr^{3+}$  ions. The quenching concentration of  $Gd_2O_2S:x\%Pr^{3+}$  phosphors is 1.00% and its corresponding CIE coordinate is (0.331, 0.564). So, the  $Gd_2O_2S:x\%Pr^{3+}$  phosphors is considered to be a promising candidate for application in the fields of green light emitting device.

### Acknowledgments

This work was supported by the Science and Technology Research Project of Department of Education of Liaoning Province (No. L2019021) and the National Natural Science Foundation of China (No. 51701090).

### References

- [1] M. Mikami, S. Nakamura, *J. Alloys Compd.* **37**(17), 687 (2006).
- [2] A. Abdelkader, M. M. Elkholy, *J. Mater. Sci. Mater. Electron.* **1**(2), 95 (1990).
- [3] M. Phamthi, A. Morell, *J. Electrochem. Soc.* **22**(24), 1100 (2010).
- [4] W. Wang, Y. S. Li, H. Kou, S. P. Liu, H. Liu, Y. Shi, J. Li, X. Q. Feng, Y. B. Pan, J. Kun, G. Wei, *J. Am. Ceram. Soc.* **98**(7), 2159 (2015).
- [5] H. Kou, S. P. Liu, W. P. Liu, Y. Shi, J. Li, X. Q. Feng, Y. B. Pan, J. K. Guo, *Int. J. Appl. Ceram. Technol.* **12**(S3), E249 (2015).
- [6] N. J. Cherepy, J. D. Kuntz, J. J. Roberts, T. A. Hurst, O. B. Drury, R. D. Sanner, T. M. Tillotson, S. A. Payne, *Proc. of SPIE.* **7079**, 70790X-1 (2008).
- [7] S. Blahuta, B. Viana, A. Bessiere, E. Mattmann, B. L. Course, *Opt. Mater.* **33**(10), 1514 (2011).
- [8] P. Liaparinos, C. Michail, I. Valais, A. Karabotsos, I. Kandarakis, *App. Phys. B (Lasers and Optics)* **128**(4), 76 (2022).
- [9] W. Wang, H. Kou, S. P. Liu, Y. Shi, J. Li, Y. S. Li, X. Q. Feng, Y. B. Pan, J. K. Guo, *Opt. Mater.* **42**, 199 (2015).
- [10] H. Yamada, A. Suzuki, Y. Uchida, M. Yoshida, H. Yamamoto, Y. Tsukuda, *Asian Pac. J. Trop. Med.* **6**(9), 691 (1989).
- [11] G. Fern, T. Ireland, J. Silver, R. Withnall, A. Michette, C. M. Faul, S. Pfauntsch, *Nucl. Instrum. Meth. B* **600**(2), 434 (2009).
- [12] J. Zhang, Z. Zhang, Z. Tang, T. Wang, *Ceram. Int.* **30**(2), 225 (2004).
- [13] J. Lian, X. Sun, G. Tie, *J. Mater. Sci. Technol.* **25**(3), 254 (2009).
- [14] Z. G. Sun, B. Lu, G. P. Ren, H. B. Chen, *Nanomaterials* **10**(9), 1639 (2020).
- [15] M. Kosari, A. Borgna, H. C. Zeng, *ChemNanoMat* **6**(2), 889 (2020).
- [16] Q. L. Dai, H. W. Song, M. Y. Wang, X. Bai, B. Dong, R. F. Qin, X. S. Qu, H. Zhang, *J. Phys. Chem. C* **112**(49), 19399 (2008).
- [17] Y. Fu, W. H. Cao, Y. Peng, X. X. Luo, M. M. Xing, *J. Mater. Sci.* **45**(23), 6556 (2010).
- [18] X. Lu, L. Y. Yang, Q. I. Ma, J. Tian, X. T. Dong, *J. Mater. Sci: Mater. Electron.* **25**(12), 5388 (2014).
- [19] S. T. Zhang, G. Q. Li, H. Y. Wang, C. Li, T. Li, Y. F. Zhang, *J. Anal. Appl. Pyrol.* **134**, 427 (2018).
- [20] H. Q. Liu, L. P. Shi, S. F. Xie, H. L. Qu, J. B. Lian, *J. Aust. Ceram. Soc.* **58**(2), 429 (2022).
- [21] Y. J. Cui, J. S. Zhang, G. Z. Zhang, J. H. Huang, P. Liu, M. Antonietti, X. C. Wang, *J. Mater. Chem.* **21**(34), 13032 (2011).

\*Corresponding author: lianjingbao@aliyun.com